

Photoluminescence Line-Shape Analysis of Highly n-Type Doped Zincblende GaN

Elias Baron,* Rüdiger Goldhahn, Michael Deppe, Donat J. As, and Martin Feneberg

An investigation of different n-type doped zincblende gallium nitride thin films measured by photoluminescence from 7 K to room temperature is presented. The spectra change with increasing free-carrier concentration due to many-body effects such as the Burstein–Moss shift and band-gap renormalization. The samples are grown by molecular beam epitaxy on a 3C-SiC/Si (001) substrate, and a free-carrier concentration above 10^{20} cm^{-3} is achieved by introducing germanium as a donor. The analysis of the measured spectra by a line-shape fit yields different transition processes for different doping concentrations and temperatures, such as a band–band transition and a band–acceptor transition. The conduction band dispersion of Kane’s model is perfectly suited to explain the experimental data quantitatively.

1. Introduction

The cubic zincblende phase of III-nitrides is often overlooked in comparison with its well-investigated hexagonal wurtzite counterpart. The zincblende III-nitrides possess intriguing properties such as a higher crystal symmetry than the wurtzite phase or the absence of spontaneous and piezoelectric polarization.^[1,2] Because of the metastable nature of the zincblende nitrides, preparation and growth are challenging. Despite that, several improvements in the layer quality of zincblende gallium nitride (zb-GaN) were recently reported.^[3–5] Furthermore, due to the higher crystal symmetry, the band structure of zb-GaN is much simpler than that of the wurtzite phase.^[6] Therefore, zb-GaN has the potential to replace wurtzite GaN in certain specific application areas such as quantum dot and quantum well-based devices.^[2,7–17]

E. Baron, Prof. R. Goldhahn, Dr. M. Feneberg
 Institut für Physik
 Otto-von-Guericke-Universität Magdeburg
 Universitätsplatz 2, 39106 Magdeburg, Germany
 E-mail: elias.baron@ovgu.de

M. Deppe, Prof. D. J. As
 Department of Physics
 University of Paderborn
 Warburger Straße 100, 33098 Paderborn, Germany

 The ORCID identification number(s) for the author(s) of this article can be found under <https://doi.org/10.1002/pssb.201900522>.

© 2019 The Authors. Published by WILEY-VCH Verlag GmbH & Co. KGaA, Weinheim. This is an open access article under the terms of the Creative Commons Attribution License, which permits use, distribution and reproduction in any medium, provided the original work is properly cited.

DOI: 10.1002/pssb.201900522

Very essential for possible applications is the understanding of the n-type doped material. To achieve free-carrier concentrations exceeding 10^{20} cm^{-3} , germanium was recently introduced as a donor instead of the standard donor silicon.^[18,19] However, for these free-carrier concentrations, the Fermi energy is pushed high into the conduction band and both the nonparabolicity of the conduction band and many-body interactions, such as band filling^[20,21] and band-gap renormalization (BGR)^[22] become increasingly important and must be considered.

Here, we perform photoluminescence (PL) on differently high-doped zb-GaN samples to determine some optical properties,

especially the effects of band filling and renormalization. We provide a comprehensive description of the measured spectra and its contributions. The used models are based on Kane’s conduction band dispersion^[23] as well as basic transitions within the band structure model.

2. Experimental Section

In this study, six samples of zb-GaN were investigated by PL measurements at different temperatures, between 7 K and room temperature (295 K). The zb-GaN layers were deposited on a 3C-SiC/Si (001) substrate by plasma-assisted molecular beam epitaxy. The samples were doped by either Ge or Si, respectively.^[19] One unintentionally doped sample (u.i.d.) was present as a reference. Spectroscopic ellipsometry measurements in the infrared, visible, and ultraviolet spectral ranges were carried out to obtain information about the zb-GaN layer thickness and free-carrier concentration. The results are shown in **Table 1**. Further information on that analysis can be found elsewhere.^[24]

The sample temperature was controlled by a helium-cooled cryostat, whereas the excitation was realized by a 266 nm continuous-wave solid-state laser (20 mW output power). The emitted light was detected by a combination of a grating monochromator (1200/mm grating density) with high focal length and a liquid nitrogen-cooled charge-coupled device camera.

3. Theory

A line-shape analysis was performed to describe the measured PL spectra close to the band gap. It has to be differentiated between degenerately doped samples (D, E, F) and samples with

Table 1. Sample properties measured by spectroscopic ellipsometry and PL: zb-GaN layer thickness d_{SE} and free-carrier concentration measured by spectroscopic ellipsometry n_{SE} at room temperature and PL n_{PL} at a low temperature.

Sample	Doping	d_{SE} [nm]	n_{SE} (at 295 K) [cm^{-3}]	n_{PL} (at 7 K) [cm^{-3}]
A	–	605	–	–
B	Ge	602	2.70×10^{18}	4.0×10^{17}
C	Si	611	7.79×10^{18}	7.0×10^{17}
D	Si	569	2.75×10^{19}	9.0×10^{18}
E	Ge	416	5.58×10^{19}	3.5×10^{19}
F	Ge	352	1.78×10^{20}	1.1×10^{20}

low doping (A, B, C). For nondegenerate doping samples, the PL spectrum is dominated by an exciton contribution (X) and a donor–acceptor pair transition (D^0A^0). The line shapes of both contributions are described as Gaussian functions. The energy position of D^0A^0 can be estimated by a Coulomb model^[25]

$$E_{D^0A^0} = E_G - E_D - E_A + \frac{e^2}{4\pi\epsilon_0\epsilon_s} \left(\frac{4\pi n}{3} \right)^{1/3} \quad (1)$$

with $(3/4\pi n)^{1/3} = R$ as the distance between the donor and acceptor.^[26] Here, $E_G = 3.295 \text{ eV}$ ^[26] is the fundamental band gap at low temperatures. The donor and acceptor binding energies are represented by E_D and E_A , respectively. In the Coulomb term, n is the free-carrier concentration and ϵ_s is a static dielectric constant dependent on the material. For zb-GaN, this value is 9.44.^[26]

The PL spectrum of degenerately doped samples displays a conduction band–to–valence band transition. For this, the model line shape derives from the multiplication of the density of states $D(E)$ and the Fermi–Dirac distribution $f_e(E)$. To achieve better results, the model line shape is also broadened by a Gaussian function. The density of states can be written as

$$D(E) = \frac{1}{\pi^2} k^2 \frac{\partial k}{\partial E} \quad (2)$$

where k and the differential come from the Kane conduction band dispersion^[23,27]:

$$E_{CB}(k) = \frac{\hbar^2 k^2}{2m_e} + \frac{1}{2} \left(E_G + \sqrt{E_G^2 + 4P^2 k^2} \right) \quad (3)$$

with the free-electron mass m_e and the momentum matrix element P . It should be noted that Equation (3) only applies for the case of the negligible spin-orbit splitting of the valence bands ($\Delta_{so} \ll E_G$). P can be determined by looking at the effective mass at the Γ point of the Brillouin zone for the undoped material at room temperature (band mass $m_0^*(\Gamma)$)^[24,28]

$$E_P = \frac{2m_e}{\hbar^2} P^2 = E_G^{RT} \left(\frac{m_e}{m_0^*(\Gamma)} - 1 \right). \quad (4)$$

Here, $E_G^{RT} = 3.23 \text{ eV}$ ^[26] is the band gap at room temperature. E_P is established as a more suitable value for discussions,

because of its energy dimension. The reported band mass of $m_0^*(\Gamma) = 0.19 m_e$ ^[28–30] yields $E_P = 13.77 \text{ eV}$.

Furthermore, the many-body effect of BGR, which describes a decrease in the band gap due to electron–electron ($\Delta E_{ee}(n)$) and electron–ion ($\Delta E_{ei}(n)$) interactions, was taken into account.^[22,27] The renormalized band gap E_{ren} can then be written as^[31,32]

$$E_{ren}(n) = E_G - \Delta E_{ee}(n) - \Delta E_{ei}(n). \quad (5)$$

Consequently, we replaced E_G with E_{ren} in Equation (3). The interaction contributions are analytically approximated by^[22]

$$\Delta E_{ee}(n) = \frac{e^2 k_F}{2\pi^2 \epsilon_0 \epsilon_s} + \frac{e^2 k_{TF}}{8\pi \epsilon_0 \epsilon_s} \left[1 - \frac{4}{\pi} \arctan \left(\frac{k_F}{k_{TF}} \right) \right] \quad (6)$$

$$\Delta E_{ei}(n) = \frac{e^2 n}{\epsilon_0 \epsilon_s a_B k_{TF}^3}. \quad (7)$$

Here, k_{TF} is the Thomas–Fermi screening vector, a_B is the effective Bohr radius (both given in Equation (8)).

$$k_{TF} = \sqrt{\frac{4k_F}{\pi a_B}}, \quad a_B = \frac{4\pi \epsilon_0 \epsilon_s \hbar^2}{m^* e^2} \quad (8)$$

Both the BGR and the transition energy are determined by the Fermi vector $k_F = (3\pi^2 n)^{1/3}$. In PL, the band–band transition occurs between the filled conduction band and the valence band maximum for degenerately doped materials. Therefore, the highest transition energy is equal to the Fermi energy $E_F = E_{CB}(k_F)$. The blue shift of this energy with increasing carrier concentration due to phase-space filling of the conduction band is known as the Burstein–Moss shift (BMS).

The model line shape is fitted on to the PL line shape by varying various parameters, especially the free-carrier concentration. The resulting carrier concentrations n_{PL} for the low-temperature experiments are shown in Table 1.

4. Results

In this section, we present both the experimental data and our model analysis. The analysis of the u.i.d. sample as well as sample D will be given in more detail as examples for the difference between the low- and high-doping analyses. Furthermore, due to the absence of free carriers, the u.i.d. sample is suitable to determine the acceptor level.

First, the data of all six samples at low temperatures (7 K) as well as a model fit are shown in **Figure 1**. The change in the spectra is clearly visible for increasing carrier concentration, corroborating BMS and BGR. The low-doped and u.i.d. samples show D^0A^0 and an X contribution, whereas the degenerately doped samples display broader spectra from band–band transitions. The model fits are according to the description in Section 3. Furthermore, samples B and C display longitudinal optical (LO) phonon replicas of the D^0A^0 transition at ≈ 3.06 and $\approx 3.11 \text{ eV}$, respectively.

We now take a closer look at the u.i.d. sample A in **Figure 2**. Here, we are able to determine three contributions to the spectra. First, we observe an exciton at 3.26 eV, which in combination with a reported exciton binding energy of $(25 \pm 1) \text{ meV}$ ^[26,33] yields a localization energy of $(12.5 \pm 1) \text{ meV}$. Therefore, we

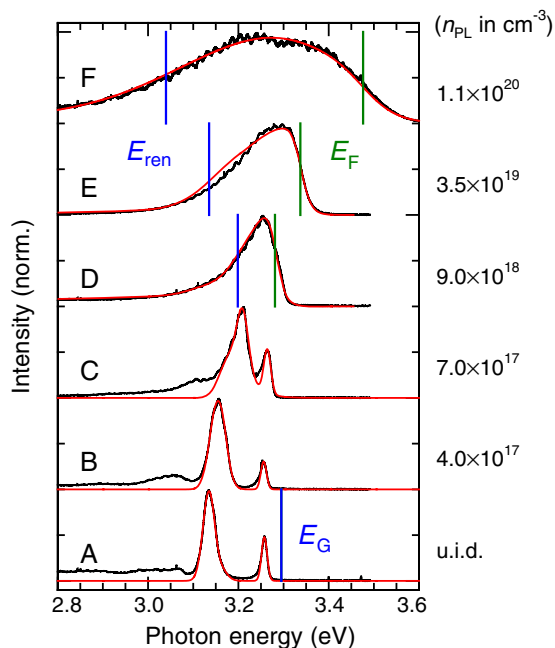


Figure 1. Experimental data (black) and model fit (red) of all samples at low temperatures (7 K). Furthermore, the calculated Fermi energy E_F (green) and renormalized band gap E_{ren} (blue) are marked as vertical lines. In addition, the used carrier concentrations are given on the right side. For clarity, the spectra are normalized to the maximum of each curve and shifted vertically.

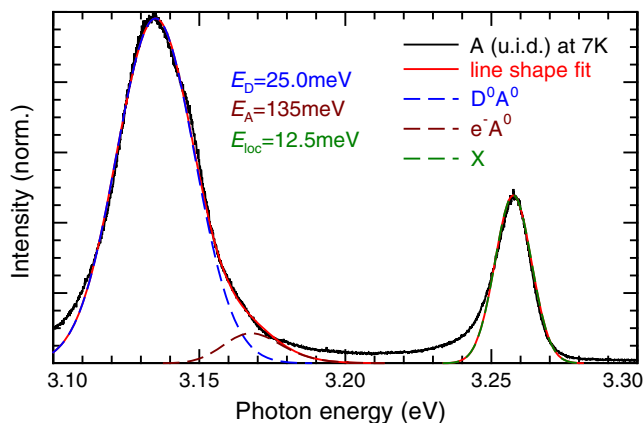


Figure 2. Experimental data (black, continuous) and model fit (red, continuous) of sample A at a low temperature (7 K). The line-shape model fit is a combination of three contributions: exciton (X, dark green, dashed), donor-acceptor pair transition (D^0A^0 , blue, dashed), and conduction band-acceptor transition (e^-A^0 , dark red, dashed). The combination of band gap, D^0A^0 and e^-A^0 , yields the donor and acceptor levels E_D and E_A , respectively. The exciton localization energy E_{loc} is determined by an exciton binding energy of 25 meV.^[33]

are mainly concerned with a bound exciton transition here. At lower energies, we see the line shape of two combined contributions. The main contribution is the D^0A^0 transition at 3.14 eV. On the high-energy wing of that peak, we find a very weak shoulder, which we determine to be a conduction band-acceptor transition (e^-A^0).^[34,35] The position of e^-A^0 at 3.16 eV as well as the

D^0A^0 position are in agreement with previous studies.^[26,30,36,37] We describe the line shape of this contribution by the same model as the line shapes for the high-doping samples ($D(E) \times f_e(E)$). The broadening by a Gaussian function is also present. A schematic description of the different transition is shown in **Figure 3**.

The position of the e^-A^0 transition can be used to determine the acceptor level $E_A = E_G - E_{e^-A^0}$, which is also in agreement with previous studies.^[26,36] In the next step, the donor level is calculated by utilizing Equation (1). In the case of the u.i.d. sample, the Coulomb term is estimated to be zero. We determine an acceptor level of $E_A = 135$ meV and a donor level of $E_D = 25$ meV, which is in agreement with previous studies.^[26,36]

Now, we exemplarily discuss the temperature-dependent PL spectra of the highly doped sample D in detail (**Figure 4**). The temperature ranges from 7 K to room temperature (295 K). For an increasing sample temperature, the spectra become broader and the determined free-carrier concentration increases. This is explained by a further activation of carriers by increasing thermal energy. Furthermore, there seems to be an energy shift to lower energies which is stronger than the BGR. This indicates that there are actually two transitions contributing to these spectra. First, there obviously is the conduction band-to-valence band transition. Second, there is a conduction band-to-acceptor transition visible as the low-energy replica of the band-band transition, shifted by the acceptor binding energy. The model line shapes of both contributions are allowed to have different broadenings in our fitting procedure. At low temperatures, the spectra are sufficiently described by the band-band transition, and nearly no band-acceptor transition is detectable. However, with increasing temperature, the band-band transition becomes weaker, whereas the band-acceptor transition remains stable, up to 100 K, where the band-acceptor transition is actually the dominant process. This can be explained by the transfer of excitation-induced holes from the valence band into the acceptor level. In the degenerately doped material, most acceptors should be neutralized by electrons from the conduction band or the donors. If generated holes are present on the acceptor level, a band-acceptor transition can occur. Here, apparently, a thermal barrier has to be overcome by photogenerated holes before they are able to reach the energetically favorable acceptor states.

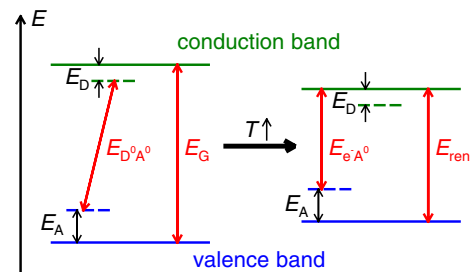


Figure 3. A schematic overview of the transitions and energy levels at a low (left) and high (right) temperature T . The increasing of T causes a decrease in the band gap (E_G) and renormalized band gap (E_{ren}) for degenerately doped samples, respectively. Furthermore, the donor-acceptor pair transitions ($E_{D^0A^0}$) evolve more to a band-acceptor transition ($E_{e^-A^0}$) for high temperatures, whereas the donor and acceptor binding energies (E_D , E_A) remain temperature independent.

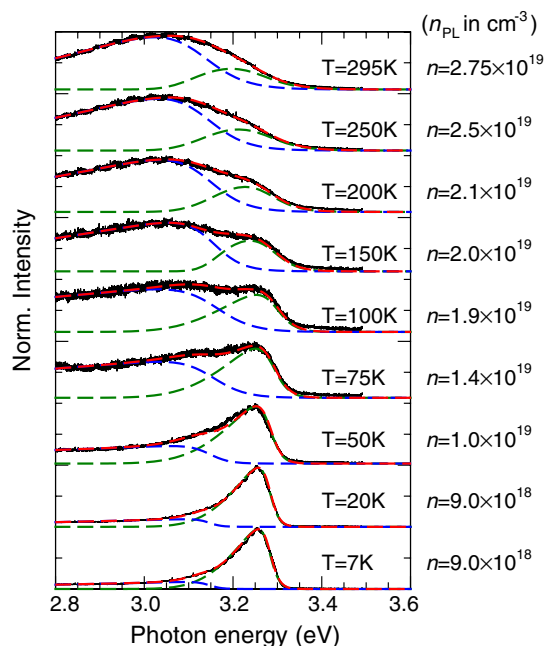


Figure 4. Temperature series of sample D. Measurement data (black, continuous), band–band transition (green, dashed), band–acceptor transition (blue, dashed), and combined model fit (red, dashed). In addition, the determined free-carrier concentrations are given on the right side. For clarity, the spectra are normalized to the maximum of each curve and shifted vertically.

The intensity behavior of both the band–band and the band–acceptor transitions in dependence on temperature is shown in **Figure 5**. There, an initial decrease in the intensity is found. However, a reactivation occurs at higher temperatures which yields an increasing intensity. Although we unfortunately cannot provide a suitable explanation of this at the moment, this

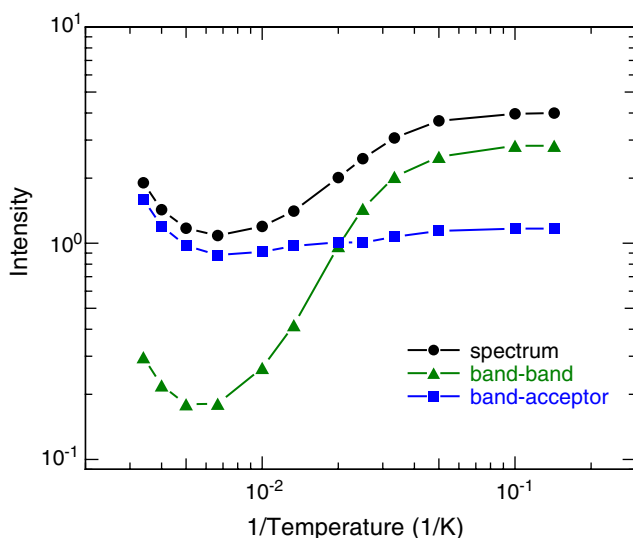


Figure 5. Intensity behavior of the experimental data (black) as well as the two transition contributions (band–band in green and band–acceptor in blue) in sample D dependent on the inverse temperature.

behavior was observed before.^[38] The literature suggests that the intensity will decline again for further increasing temperatures.

In conclusion, the D^0A^0 and X contributions disappear with increasing free-carrier concentration (see Figure 1), due to the increasing effect of band filling and many-body interactions, and therefore band–band transitions are observed at high concentrations and low temperatures. Furthermore, the e^-A^0 transition in degenerately doped samples seems to remain more or less stable, independent of free-carrier concentration or temperature.

5. Conclusion

In this study, we investigated samples of differently high-doped zb-GaN by PL from 7 K to room temperature. The change of the spectra dependent on free-carrier concentration and on temperature is described by means of BMS and BGR. Furthermore, the analysis of an u.i.d. reference sample at a low temperature leads to the determination of the donor and acceptor levels, as well as the exciton localization energy. The temperature series of a degenerately doped sample indicates a shift from a band–band transition to a band–acceptor transition with increasing temperature.

Acknowledgements

The authors gratefully acknowledge support by the Deutsche Forschungsgemeinschaft in the framework of Major Research Instrumentation Programs no. INST 272/230-1 and via project B02 within the Transregio program TRR 142, project number 231447078.

Conflict of Interest

The authors declare no conflict of interest.

Keywords

band filling, GaN, photoluminescence

Received: August 27, 2019

Revised: October 22, 2019

Published online: November 8, 2019

- [1] L. Shunfeng, J. Schörmann, D. J. As, K. Lischka, *Appl. Phys. Lett.* **2007**, *90*, 071903.
- [2] M. T. Durniak, A. S. Bross, D. Elsaesser, A. Chaudhuri, M. L. Smith, A. A. Allerman, S. C. Lee, R. J. Brueck, C. Wetzel, *Adv. Electron. Mater.* **2016**, *2*, 1500327.
- [3] L. Y. Lee, *Mater. Sci. Technol.* **2017**, *33*, 1570.
- [4] R. Liu, R. Schaller, C. Q. Chen, C. Bayram, *ACS Photonics* **2018**, *5*, 955.
- [5] L. Y. Lee, M. Frentrup, M. J. Kappers, R. A. Oliver, C. J. Humphreys, D. J. Wallis, *J. Appl. Phys.* **2018**, *124*, 105302.
- [6] M. Feneberg, M. Winkler, K. Lange, M. Wieneke, H. Witte, A. Dadgar, R. Goldhahn, *Appl. Phys. Express* **2018**, *11*, 101001.
- [7] S. Kako, M. Miyamura, K. Tachibana, K. Hoshino, Y. Arakawa, *Appl. Phys. Lett.* **2003**, *83*, 984.
- [8] M. Bürger, T. Schupp, K. Lischka, D. J. As, *Phys. Status Solidi C* **2012**, *9*, 1273.

- [9] M. Bürger, M. Ruth, S. Declair, J. Förstner, C. Meier, D. J. As, *Appl. Phys. Lett.* **2013**, *102*, 081105.
- [10] C. J. M. Stark, T. Detchprohm, S. C. Lee, Y.-B. Jiang, S. R. J. Brueck, C. Wetzel, *Appl. Phys. Lett.* **2013**, *103*, 232107.
- [11] S. Sergent, S. Kako, M. Bürger, T. Schupp, D. J. As, Y. Arakawa, *Phys. Rev. B* **2014**, *90*, 235312.
- [12] S. Kako, M. Holmes, S. Sergent, M. Bürger, D. J. As, Y. Arakawa, *Appl. Phys. Lett.* **2014**, *104*, 011101.
- [13] M. Bürger, J. K. N. Lindner, D. Reuter, D. J. As, *Phys. Status Solidi C* **2015**, *12*, 452.
- [14] T. Wecker, F. Hörich, M. Feneberg, R. Goldhahn, D. Reuter, D. J. As, *Phys. Status Solidi B* **2015**, *252*, 873.
- [15] S. Sergent, S. Kako, M. Bürger, S. Blumenthal, S. Iwamoto, D. J. As, Y. Arakawa, *Appl. Phys. Express* **2016**, *9*, 012002.
- [16] T. Wecker, G. Callsen, A. Hoffmann, D. Reuter, D. J. As, *Jpn. J. Appl. Phys.* **2016**, *55*, 05FG01.
- [17] S. Blumenthal, D. Reuter, D. J. As, *Phys. Status Solidi B* **2018**, *255*, 1700457.
- [18] M. Deppe, J. W. Gerlach, D. Reuter, D. J. As, *Phys. Status Solidi B* **2017**, *254*, 1600700.
- [19] M. Deppe, J. W. Gerlach, S. Shvarkov, D. Gogalla, H.-W. Becker, D. Reuter, D. J. As, *J. Appl. Phys.* **2019**, *125*, 095703.
- [20] E. Burstein, *Phys. Rev.* **1954**, *93*, 632.
- [21] T. S. Moss, *Proc. Phys. Soc. B* **1954**, *67*, 775.
- [22] K.-F. Berggren, B. E. Sernelius, *Phys. Rev. B* **1981**, *24*, 1971.
- [23] E. O. Kane, *J. Phys. Chem. Solids* **1957**, *1*, 249.
- [24] E. Baron, R. Goldhahn, M. Deppe, D. J. As, M. Feneberg, *Phys. Rev. Mater.* **2019**, *3*, 104603.
- [25] P. Y. Yu, M. Cardona, *Fundamentals of Semiconductors: Physics and Materials Properties*, 4th ed., Springer, Berlin **2010**, p. 356.
- [26] M. Feneberg, M. Röppischer, C. Cobet, N. Esser, J. Schörmann, T. Schupp, D. J. As, F. Hörich, J. Bläsing, A. Krost, R. Goldhahn, *Phys. Rev. B* **2012**, *85*, 155207.
- [27] J. Wu, W. Walukiewicz, W. Shan, K. M. Yu, I. I. I. J. W. Ager, E. E. Haller, H. Lu, W. J. Schaff, *Phys. Rev. B* **2002**, *66*, 201403.
- [28] P. Rinke, M. Winkelnkemper, A. Qteish, D. Bimberg, J. Neugebauer, M. Scheffler, *Phys. Rev. B* **2008**, *77*, 075202.
- [29] L. C. de Carvalho, A. Schleife, F. Bechstedt, *Phys. Rev. B* **2011**, *84*, 195105.
- [30] J. R. L. Fernandez, O. C. Noriega, J. A. N. T. Soares, F. Cerdeira, E. A. Meneses, J. R. Leite, D. J. As, D. Schikora, K. Lischka, *Solid State Commun.* **2003**, *125*, 205.
- [31] M. Feneberg, J. Nixdorf, C. Lidig, R. Goldhahn, Z. Galazka, O. Bierwagen, J. S. Speck, *Phys. Rev. B* **2016**, *93*, 045203.
- [32] R. A. Abram, G. J. Rees, B. L. H. Wilson, *Adv. Phys.* **1978**, *27*, 799.
- [33] J. Menniger, U. Jahn, O. Brandt, H. Yang, K. Ploog, *Phys. Rev. B* **1996**, *53*, 1881.
- [34] A. Philippe, C. Bru-Chevallier, M. Vernay, G. Guillot, J. Hbner, B. Daudin, G. Feuillet, *Mater. Sci. Eng. B* **1999**, *59*, 168.
- [35] C.-W. Chen, M.-C. Wu, S.-C. Lu, C.-C. Chang, *Jpn. J. Appl. Phys.* **1993**, *32*, 2725.
- [36] D. J. As, F. Schmilgus, C. Wang, B. Schttker, D. Schikora, K. Lischka, *Appl. Phys. Lett.* **1997**, *70*, 1311.
- [37] J. H. Buß, T. Schupp, D. J. As, D. Hägele, J. Rudolph, *J. Appl. Phys.* **2019**, *126*, 153901.
- [38] I. Pelant, J. Valenta, *Luminescence Spectroscopy of Semiconductors*, 1st ed., Oxford University Press, Oxford **2012**, p. 121.